Journal of
Manufacturing and Materials Processing

MDPI

Article

Powder Metallurgical Processing of Sn-Reinforced Al-Cu-Fe Quasicrystals: Structure, Microstructure and Toughening Behavior

Yagnesh Shadangi [1,*], Vikas Shivam [1,2], Kausik Chattopadhyay [1] and Nilay Krishna Mukhopadhyay [1,*]

[1] Department of Metallurgical Engineering, Indian Institute of Technology (BHU), Varanasi 221005, India; vikasmit24@gmail.com (V.S.); kausik.met@iitbhu.ac.in (K.C.)
[2] Materials Processing Group, Materials Engineering Division, CSIR-National Metallurgical Laboratory, Jamshedpur 831007, India
* Correspondence: yshadangi.met12@iitbhu.ac.in (Y.S.); mukho.met@iitbhu.ac.in (N.K.M.); Tel.: +91-872-688-080 or +91-752-588-7370 (Y.S.); +91-983-9817585 (N.K.M.)

Abstract: The present work deals with powder metallurgical processing of Sn-reinforced Al-Cu-Fe icosahedral quasicrystalline (IQC) composites processed through mechanical milling (MM) followed by hot pressing and pressureless sintering. The structure, microstructure and toughening behavior of the nanocomposite powders and bulk samples were investigated through X-ray diffraction (XRD), optical metallography (OM), scanning electron microscopy (SEM) and indentation techniques. The XRD pattern suggested the coexistence of IQC and λ-$Al_{13}Fe_4$ (mC102; a = 1.549 nm, b = 0.808 nm, c = 1.248 nm) and B2-type Al (Cu, Fe) (cP2; a = 0.29 nm) crystalline phases in milled as well as sintered samples. The face-centered icosahedral (FCI) ordering was persistent even after 40 h of milling and sintering. The structural transformation during MM influences the indentation behavior of IQC-Sn nanocomposite powders, and the microhardness was found to be in the range of ~5.3 to 7.3 GPa. Further, efforts were made to study the indentation behavior of IQC-Sn composite prepared by pressureless sintering and hot pressing. The fracture toughness of the IQC-10Sn hot-pressed sample was found to be ~1.92 MPa. $\sqrt{m}$, which is ~22% higher than that of the as-cast and annealed IQC. The enhancement in the fracture toughness resulted mainly from the inhibition of cracks by Sn reinforcement particles. This suggests that powder metallurgical processing can produce the IQC-Sn composite with an optimal combination of microhardness and fracture toughness.

Keywords: Al-Cu-Fe quasicrystalline matrix; Sn reinforcement; mechanical milling; sintering; microhardness; fracture toughness

check for updates

Citation: Shadangi, Y.; Shivam, V.; Chattopadhyay, K.; Mukhopadhyay, N.K. Powder Metallurgical Processing of Sn-Reinforced Al-Cu-Fe Quasicrystals: Structure, Microstructure and Toughening Behavior. *J. Manuf. Mater. Process.* **2022**, *6*, 60. https://doi.org/10.3390/jmmp6030060

Academic Editor: Steven Y. Liang

Received: 17 April 2022
Accepted: 27 May 2022
Published: 31 May 2022

1. Introduction

The paradigm shift in alloy design and development strategies has led to the discovery of many fascinating materials such as quasicrystals [1], high-entropy alloys [2,3], bulk metallic glasses [4], nanostructured materials [5,6], etc. The discovery of quasicrystal (QC) in Al-Mn alloy by Shechtman et al. in 1984 challenged the conventional crystallographic concepts. It led to the discovery of aperiodic intermetallics having forbidden rotational symmetry without long-range transitional periodicity [1]. These QCs exhibit high hardness, excellent wear resistance, low coefficient of friction, good corrosion resistance and low electrical and thermal conductivity [7–11]. Researchers and coworkers have reported the presence of quasicrystalline phases in several hundred compositions synthesized by various equilibrium and nonequilibrium processing routes [12–14]. Among the known quasicrystalline compositions, ~80% contain icosahedral (I) phases and around ~80% of those I-phases have Al as the major alloying element [15]. Therefore, the Al-TM (TM = transition elements such as Cr, Mn, Co, Ni, Fe, etc.) binary and ternary alloys are studied more extensively for exploiting its potential applications [8]. Apart from the synthesis of these QCs, a few researchers have reported the existence of naturally occurring QCs [16,17]. The face-centered icosahedral (FCI) ordering in Al-Mn IQC was first reported by Mukhopadhyay et al. [18] after the discovery of simple icosahedral (SI) QC by Shechtman et al. [1], as evidenced through the presence of a (311111) and other superlattice reflections.

The impetus for the design and development of QC phases in Al-TMs binary and ternaryalloy systems has led to the discovery of icosahedral quasicrystalline (IQC) phases in Al-Cu-Fe ternary alloy by Tsai et al. [19]. The Al-Cu-Fe alloys are most widely studied due to their nontoxicity, cost-effectiveness of constituent elements and easy availability [8]. The stable IQC phases in ternary Al-Cu-Fe systems can be synthesized in the compositional range of 58–70 Al, 20–28 Cu and 10–14 Fe (in at %) [8]. During the initial days of QCs, efforts were mainly devoted to the understanding of structural and microstructural features. Of late, a few investigations have suggested inherent room-temperature brittleness in these QCs containing alloy systems [13,20]. Therefore, exploiting these quasicrystals as a monolithic structural material practically becomes impossible. However, these quasicrystals can be used as a potent material for coatings, reinforcement in metal matrix composites [21], a catalyst of hydrogen storage [22,23] and steam forming of methanol for H_2 production [24]. To overcome the problem associated with inherent room-temperature brittleness, various toughening strategies have been adopted to enhance fracture toughness and to exploit these materials for coating applications. The toughening of these quasicrystals can be performed either through nanostructuring [25,26] or by incorporation of soft particulates (such as Sn, Pb etc.) [27–29], carbon [30] or onion-like carbon (OLC) [31].

For the past three decades, researchers have made efforts to understand the synthesis and fabrication of Al-Cu-Fe IQC alloys through melting and solidification routes [7,32]. However, due to the narrow compositional range, differences in melting point and density of principal elements make the synthesis of these alloys cumbersome and challenging through liquid metallurgy routes [7]. Unlike conventional melting and solidification routes, powder metallurgical processing (i.e., mechanical alloying and milling) has been extensively used to synthesize nanostructured quasicrystals [33–38]. Many researchers and coworkers have studied Al-Cu-Fe IQC alloys by mechanical alloying and annealing treatment [33,39,40]. A few researchers have discerned the formation of B2-type Al(Cu, Fe) phases during mechanical alloying (MA) of Al-Cu-Fe elemental powders in the compositional range desired for the formation of IQC phases [33,39,40]. Further, it was observed that suitable annealing of these B2-type phases in a temperature range of ~600–800 °C resulted in stable IQC phases [33,39,40].

In contrast to the MA routes followed by suitable heat treatment, a few researchers have attempted the synthesis of nanostructured IQC phases through mechanical milling (MM) [25,36,37,41,42]. The MM of quasicrystals results in the formation of nanoquasicrystalline phases and other crystalline phases depending on milling duration and intensity [42]. Further, MM induces disordering in FCI-ordered IQC phases in Al-Cu-Fe alloys, and the extent of disordering is dependent on several external parameters such as ball-to-powder ratio (BPR), vials and balls, milling speed, etc. [42]. In an investigation, Mukhopadhyay et al. [43] showed the coexistence of nanostructured B2-type and IQC phases in a Al-Cu-Fe alloy system milled for 40 h and 20h with a milling speed of 200 and 400 r.p.m, respectively. They also observed softening and inverse Hall–Petch behavior (IHP) for nano-quasicrystalline (below ~40 nm) Al-Cu-Fe IQC alloys [25]. The preparation of IQC through MM was found to be effective in enhancing the toughness by grain softening in these kinds of alloys.

Apart from grain refinement and grain softening, many investigators have reported the incorporation of soft particles (such as Sn or Pb), or carbon into the quasicrystalline matrix [30,31,44,45]. They have investigated the incorporation of the soft reinforcement phases in the Al-Cu-Fe IQC matrix through melt spinning [28], conventional melting and solidification routes [44] and spray forming [20]. During the melt spinning of Sn containing Al-Cu-Fe IQC matrix, a few researchers observed the formation of faceted interfaces [46]. Fleury et al. [44] discerned the enhancement in the fracture toughness for Al-Cu-Fe and Al-Cu-Fe-B IQC alloys reinforced with 10 vol% of Sn reinforcement. They further reported an increase in the compressive strength to ~130% and 90% for Al-Cu-Fe and Al-Cu-Fe-B

IQC alloys, respectively. The fracture toughness and compressive-strength enhancement were observed for up to 15 vol% of Sn reinforcement. However, there was no significant increase in fracture toughness and compressive strength for IQC composites with 20 vol% or more. Shao et al. [45] observed excellent wear resistance of Sn-reinforced IQC composites coated on the surface of medium carbon steel.

Further, Mukhopadhyay and coworkers have made systematic efforts to enhance the fracture toughness of these IQC alloys by incorporating Sn reinforcement in the IQC matrix by spray forming [47]. Srivastava et al. [20] discerned the enhancement in the fracture toughness of these composites through inhibition of cracks by soft Sn particles. However, an increase in the fracture toughness of these Al-Cu-Fe IQC reinforced with 10 wt% of Sn is associated with a nominal decrease in microhardness (~6.0 GPa). Although a significant enhancement in fracture toughness resulted in these kinds of composites, the homogenous distribution of Sn in the IQC matrix remains a challenging task through melting and solidification routes. It is evident from the previous investigation that the toughening of these Al-Cu-Fe IQCs can be attempted either through mechanical milling or by the incorporation of soft phases.

In contrast to the previous studies, we recently reported the synthesis of the Sn-reinforced Al-Cu-Fe IQC composites through MM [48,49] and discerned the details of the mechanically driven transformation during milling [49]. The synthesis of this nanocomposite by MM was a very efficient method for the homogenous distribution of Sn particles in the IQC matrix. However, in our previous investigations no attempts were made towards studying the toughening behavior and sintering of IQC-Sn composites. Therefore, in the present investigation efforts were made to establish the influence of structural transformation during MM on the microhardness and toughening behavior of Sn-reinforced Al-Cu-Fe IQC nanocomposite powders. Further, sincere attempts were made to study the effect of Sn reinforcement on structure, microstructure, indentation behavior and fracture toughness of IQC-Sn bulk composites fabricated through pressureless sintering and hot pressing.

2. Experimental Details

The as-cast $Al_{62.5}Cu_{25}Fe_{12.5}$ (at%) IQC alloy was prepared under Ar gas in a vacuum induction melting (VIM) unit. These as-cast alloys were annealed at 800 °C (1073 K) for 4 h followed by crushing into smaller pieces, and will be referred as IQC-AA (Table S1). The Sn particles (~325 mesh size) with a purity of 99.90% were used for reinforcement into the $Al_{62.5}Cu_{25}Fe_{12.5}$ (at %) IQC-AA alloys. The composites are IQC-10Sn, IQC-20Sn and IQC-30Sn were reinforced with 10, 20 and 30 vol% of Sn, respectively (Table S1). The IQC-Sn nanocomposites were synthesized by mechanical milling for 40 h for homogenous distribution of Sn reinforcement. The MM was performed at 200 r.p.m in WC vials and balls (10 mm diameter) with toluene as a process-control reagent. The milling was carried out for 30 min followed by 15 min rest to avoid overheating. The IQC-Sn milled powder was withdrawn after every 10 h of MM.

The IQC-Sn nanocomposites prepared by milling were consolidated by pressureless sintering and hot-pressing. For pressureless sintering of IQC-Sn composites, green pellets of 40 h milled samples were sealed in a quartz tube back-filled with Ar gas [50–52]. The green pellets of IQC-Sn nanocomposite powders were prepared by cold pressing. The IQC-Sn 40 h milled powder (~5–6 g) was placed inside a steel die of 12 mm inner diameter and compacted at a load of 5 ton. The pressureless sintering was performed at 800 °C (1073 K) for 10 h. The IQC-10Sn nanocomposite powders were additionally sintered through hot pressing. The die made up of H13 die steel of 10 mm diameter was fabricated for this particular purpose. The die cavity, bottom and upper punch were coated with a thin boron nitride (BN) layer to avoid powder sticking to die during sintering. The 40 h mechanically milled nanocomposite powder of IQC-10Sn (5–6 g) was placed inside the die and was kept in the hydraulic press with the resistance furnace (100-Ton capacity; Crane-Bel International Pvt. Ltd., Ghaziabad, India). The resistance-heating method was used to obtain the desired temperature during hot pressing. The sample was hot-pressed at 650 °C (923 K) at a pressure of 650 MPa for 15 min in an ambient atmosphere. The sintered pellets had a thickness of 4–5 mm. These hot-pressed samples were further annealed at 800 °C for 4 h. The Archimedes principle was used to measure the density of sintered pellets of IQC-Sn bulk composite. The density of sintered samples ρ(sample) was calculated by Equation (1):

$$\rho(\text{sample}) = \frac{m(\text{air})[\rho(\text{liquid}) - \rho(\text{air})]}{m(\text{air}) - m(\text{liquid})} \quad (1)$$

where ρ(liquid) is the density of the liquid medium, ρ(air) is the density of air, m(air) is sample weight in ambiance, and m(liquid) is the weight of the sample immersed in the liquid medium. The samples were first measured in air and then in a liquid medium using an electronic weighing balance (Model No- CAH-503, CONTECH Instrument Ltd., Mumbai, India) equipped with a density-measurement module. Further, the relative density of the samples was calculated by Equation (2):

$$\text{Relative density } (\%) = \frac{\rho(\text{experimental})}{\rho(\text{theoretical})} * 100 \quad (2)$$

The nanocomposite powders and bulk composite's detailed structural, microstructural and indentation behavior were characterized through X-ray diffraction (XRD), SEM-EDS, microhardness tester (HMV-2; Make: Shimadzu Corporation, Kyoto, Japan). The details of parameters for XRD and SEM-EDS are described elsewhere [48,49]. The IQC-Sn nanocomposite powders were embedded in epoxy resin, followed by mirror polishing for indentation. The indentation of IQC-Sn nanocomposite powders was carried out at a load of 10 g. For each sample, at least ten (10) readings were taken to compute the average reading and standard deviation. The details of the sample designation and its processing conditions are mentioned in the Supplementary Table (Table S1).

3. Results

The powder XRD pattern shown in Figure 1a,b gives an insight into the phase formation in the as-cast IQC (followed by annealing at 800 °C (1073 K) for 4 h) and in Sn reinforcement particles, respectively. The XRD pattern (Figure 1a) discerns the presence of IQC phases as evident from its major reflection, i.e., (222000) (d~3.748 Å), (311111) (d~3.415 Å), (22202$\bar{2}$0) (d~3.224 Å), (400222) (d~2.456 Å), (422222) (d~2.111 Å), (244020) (d~2.007 Å) & (4660$\bar{4}$0) (d~1.240 Å). The stable IQC phases formed in the present investigation were found to be ordered IQC or face-centered IQC, as evident from the presence of the (311111) reflection. The coexistence of crystalline phases such as λ-$Al_{13}Fe_4$ (JCDPS card no.: 65–1257; a = 1.548 nm, b = 0.80831, c = 1.2476 nm) and B2-type Al (Cu, Fe) (JCPDS card no.: 65–3201; a = 0.29 nm; cP2) phases, along with IQC phases, was also evident from the Figure 1a. The phase fractions of IQC, λ-$Al_{13}Fe_4$ and B2-type Al(Cu, Fe) phases were found to be ~84%, 12% and 4%, respectively. From the XRD pattern shown in Figure 1b, it is evident that all the major reflections of Sn reinforcement particles correspond to β-Sn (i.e., (200), (101), (220), (211)) having a tetragonal crystal structure (JCPDS data card no.: 00-004-0673; a = b = 0.58 nm, c = 0.3182 nm; tI4). Further, the morphologies of the crushed IQC alloys and Sn reinforcement particles are shown in Figure 1c,d, respectively. From Figure 1c, it is clear that the average size of the crushed IQC particles was ≤50 μm and had faceted morphology. Similarly, the Sn reinforcement particle used in the present investigation had quasi-spherical morphology and a few particles also had elongated morphology, as observed in Figure 1d.

Figure 2a–c show the structural transformation of IQC-10Sn, IQC-20Sn and IQC-30Sn milled up to 40 h. From Figure 2 it can be discerned that the structural transformation of IQC into crystalline phases is dependent upon the volume fraction of Sn, and also the duration of MM. However, the phase fraction of the crystalline phases increases upon increasing the milling duration up to 40 h for IQC-Sn nanocomposites. Figure 2a shows that the phase fraction of the λ-$Al_{13}Fe_4$ phase is more than the B2-type and IQC phases.

Further, disordering in the FCI IQC was also observed due to milling up to 40 h. However, the case was not same for the IQC-20Sn nanocomposites powder.

From Figure 2b, it was evident that the phase fraction of the B2-type phase increases in comparison to the λ and IQC phases. Despite the increase in the B2-type phase, the IQC matrix retained its ordering, as evident from the existence of the (311,111) reflection of the IQC phase. Figure 2c discerns the structural transformation during milling of IQC-30Sn. It was evident from Figure 2c that the phase fraction of B2-type phases increases considerably in contrast to the IQC phase. After milling, the phase fraction of the λ phases was not very appreciable, as observed in IQC-10Sn and IQC-20Sn. Similar to IQC-20Sn, the IQC phases in IQC-30Sn retained their face-centered ordering, as evident from the (311,111) reflection shown in Figure 2c. During MM of IQC-Sn nanocomposite powder, Sn particles did not undergo any structural transformations, as evident from Figure 2. The details for the structural transformation and grain refinement during mechanical milling of IQC-Sn nanocomposites are described in our previous articles [48,49].

Figure 3 shows the variation of microhardness of IQC-Sn nanocomposite powder concerning the duration of MM. It was observed that the microhardness of IQC-Sn nanocomposite powder increases with the duration of milling up to 40 h. The peak microhardness observed for IQC-10Sn, 20Sn, and 30Sn was found to be 7.3 ± 0.22 GPa, 6.4 ± 0.28 GPa, and 5.25 ± 0.11 GPa, respectively. The increase in the microhardness from 20 h to 30 h of MM is not very significant as compared to 10–20 h and 30–40 h. These results are in line with the structural transformation in IQC-Sn nanocomposites, as shown in Figure 2. It was also observed that the microhardness tends to decrease upon increasing the volume fraction of Sn reinforcement in the IQC matrix (Table 1).

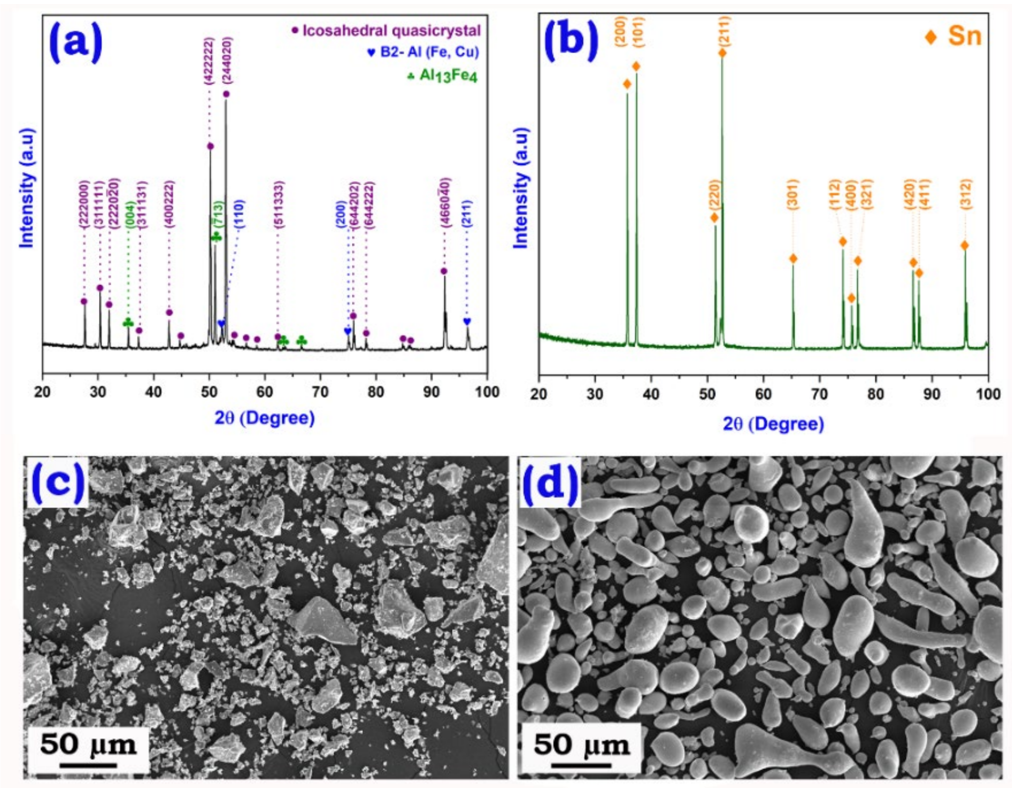

Figure 1. Phase analysis of (**a**) as-cast and annealed IQC alloys (IQC-AA) and (**b**) Sn reinforcement particles. SEM micrograph showing the morphology and size of (**c**) as-cast and annealed IQC alloys (IQC-AA) and (**d**) Sn particles.

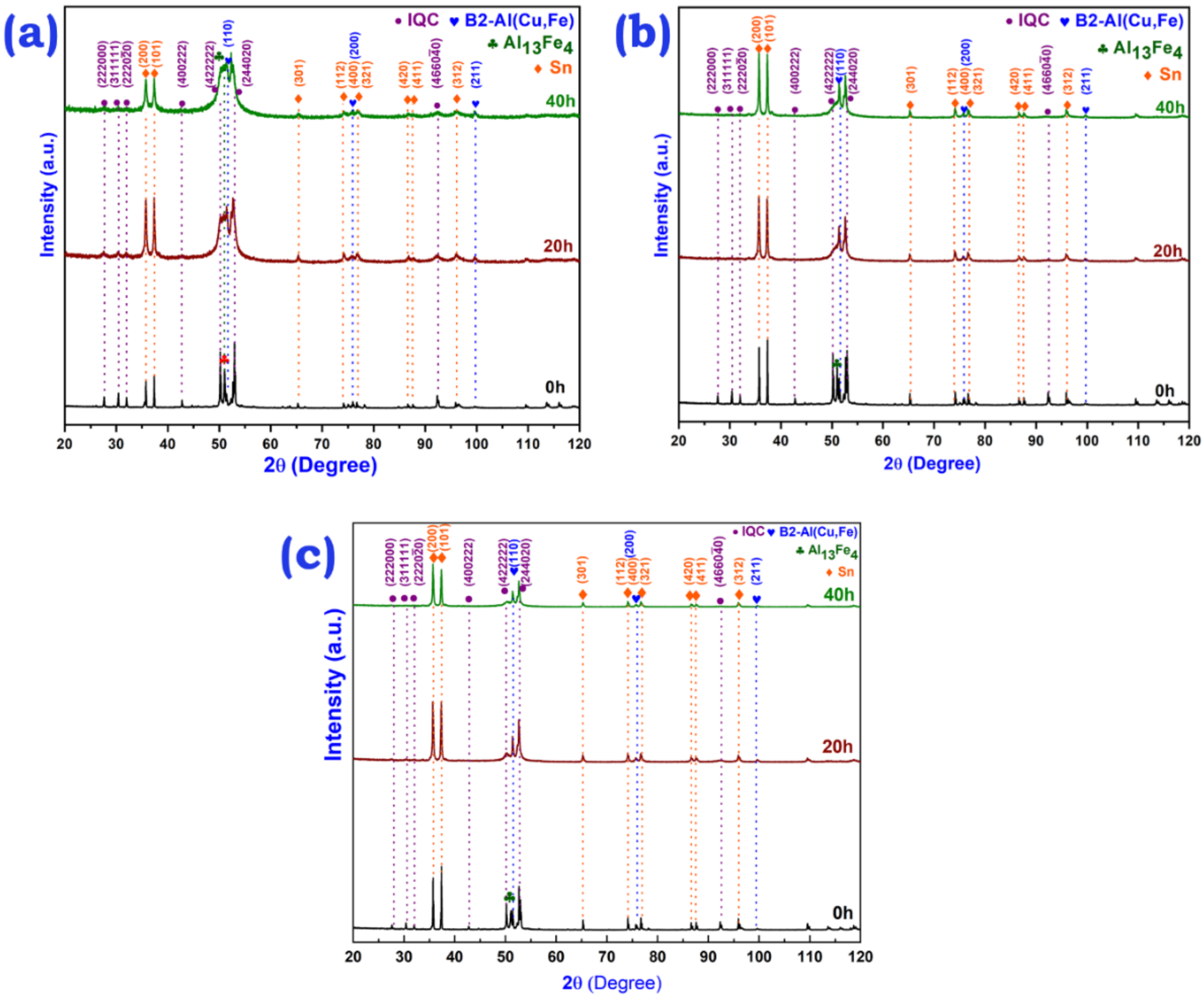

Figure 2. Phase analysis of (**a**) IQC-10Sn, (**b**) IQC-20Sn and (**c**) IQC-30Sn nanocomposite powders mechanically milled up to 40 h.

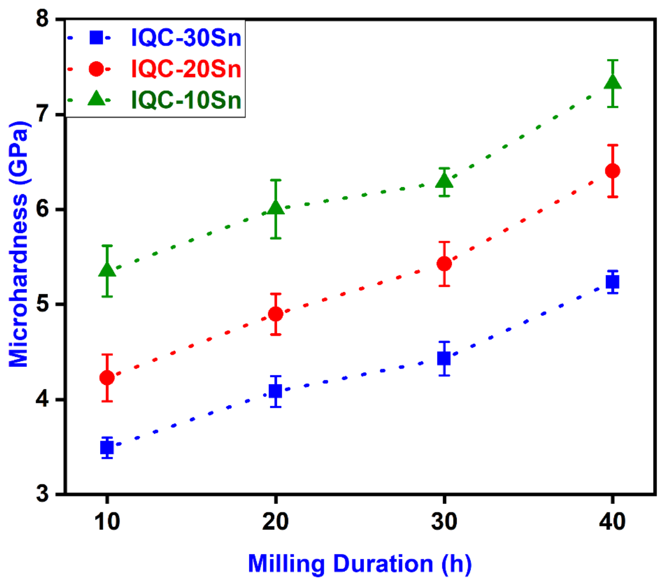

Figure 3. Microhardness (at an indentation load of 10 g) of IQC-Sn nanocomposite powders as a function of the duration of mechanical milling.

Table 1. Microhardness of IQC-Sn nanocomposite powder samples.

Sample Condition	Microhardness (GPa)		
	Sample Designation		
	IQC-10Sn	IQC-20Sn	IQC-30Sn
10 h MM	5.2	4.2	3.5
20 h MM	6.0	4.9	4.1
30 h MM	6.3	5.4	4.4
40 h MM	7.3	6.4	5.3

The optical micrographs of Figure 4 show the indentation marks of the 20 h and 40 h MM powders of IQC-10Sn, IQC-20 Sn, and IQC-30Sn. It can be discerned from Figure 4a–f that the crack length after indentation at a load of 10 g is highest for IQC-10Sn, followed by IQC-20Sn and 30Sn. The inhibition of cracks during indentation varies as a function of the volume fraction of Sn and the duration of MM. Upon increasing the time of MM to 40 h, the crack length of IQC-10Sn, 20Sn and 30Sn after indentation decreases, as shown in Figure 4b,d,f, respectively. After 40 h of MM, no significant marks of indentation cracks were observed for IQC-10Sn, 20Sn and 30Sn nanocomposite powder. However, the case for 20 h MM IQC-Sn nanocomposite powder is not the same. The crack lengths for 20 h MM IQC-10Sn, 20Sn and 30Sn were found to be ~11.5 μm, ~6.5 μm, and ~4.2 μm, respectively.

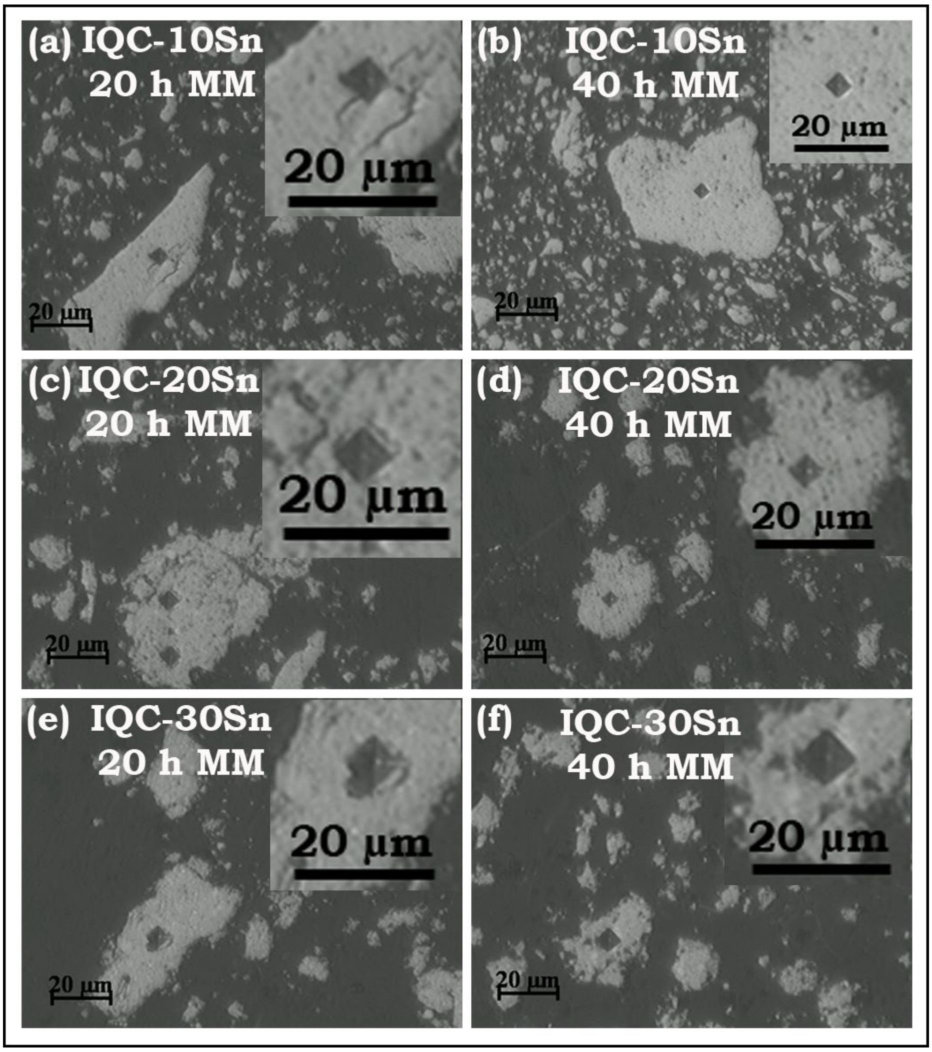

Figure 4. Optical micrograph showing indentation marks on the (**a**,**b**) IQC-10Sn, (**c**,**d**) IQC-20Sn and (**e**,**f**) IQC-30 Sn nanocomposite powder MM for 20 h and 40 h.

The IQC-Sn nanocomposite powders were consolidated using pressureless sintering (usually referred to as conventional sintering) at 800 °C (1073 K) for 10 h. The phase formation in IQC-10Sn-PS and IQC-30Sn-PS pressureless-sintered samples can be ascertained through the XRD pattern shown in Figure 5. The phases formed in the IQC-20Sn-PS were similar to the IQC-30Sn-PS. Therefore, the XRD pattern pertaining to IQC-10Sn-PS and IQC-30Sn-PS were only shown in the Figure 5. It is clear from the XRD pattern that the IQC phase retained its identity even after pressureless sintering, as evident from the presence of all the major reflections of the IQC phase. The IQC phases in IQC-Sn were found to be FCI IQC, as evidenced by the presence of the (311111) peak shown in Figure 5. The IQC matrix partially transforms to a minor amount of λ and B2-type phases during sintering. The presence of the λ-$Al_{13}Fe_4$ phase can be confirmed through the presence of the major reflection $(\bar{7}13)$ at d~2.0778 Å, as shown in the Figure 5. The peak intensity of $(\bar{7}13)$ at d~2.0778 Å of the $Al_{13}Fe_4$ phase is higher for IQC-10Sn-PS than for IQC-30Sn-PS. Similarly, the presence of B2-type phases in the IQC-Sn pressureless-sintered composite was ascertained through the presence of (110) and (200) major peaks at d~2.056 Å and d~1.447 Å, respectively. The intensity of the B2-type phase is more in comparison to the λ-phase in IQC-30Sn-PS. The phase fraction of the λ-phase is more comparable to the B2-type phase in IQC-10Sn-PS. The ordering of the B2-type phase will be difficult to ascertain through XRD. The (100) superlattice reflection of the B2-type phase at d~2.90 Å coincides with Sn's (200) reflection at d~2.91 Å. However, in IQC-30Sn-PS, the phase fraction of the B2-type phase is relatively higher than the λ-phase. The Sn reinforcement in the IQC matrix has not undergone any phase transformation or reaction and was found to be independent of the volume fraction Sn. All the major reflections, i.e., (200), (101), (220), (211) corresponding to the β-Sn were present in IQC-Sn pressureless-sintered samples.

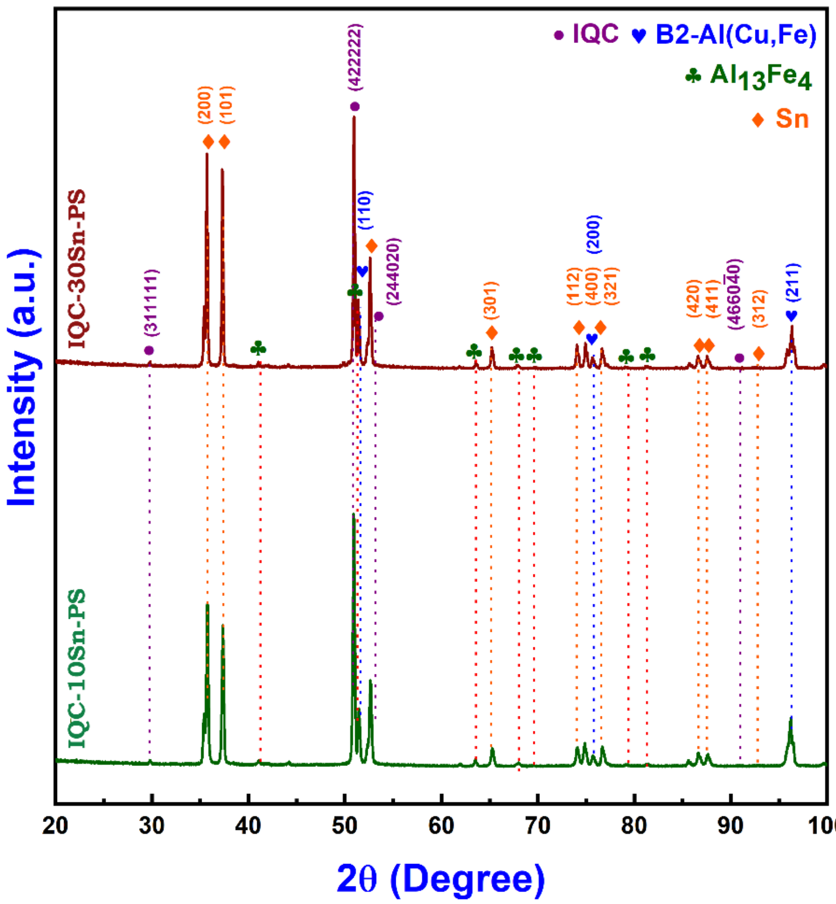

Figure 5. Phase analysis of IQC-Sn composites pressureless-sintered (IQC-10Sn-PS and IQC-30Sn-PS) at 800 °C (1073 K) for 10 h.

The microstructural details of the pressureless-sintered IQC-Sn composites are revealed through SEM micrograph, shown in Figure 6. The SEM micrograph depicts the fine microstructural details of the IQC-10Sn-PS (Figure 6a,b), IQC-20Sn-PS (Figure 6c,d), IQC-30Sn-PS (Figure 6e,f) composites in back-scattered mode. It was observed that the micrograph has particles corresponding to light-grey, dark-grey and bright contrast. The light-grey contrast corresponds to the IQC and B2-type phases, whereas the dark-grey contrast corresponds to the λ-phase, and the bright contrast corresponds to the Sn reinforcement. Therefore, it is clear from Figure 6 that the Sn particles are uniformly distributed in the IQC matrix containing other crystalline phases. It can further be revealed that the phase fraction of the λ-phase decreases upon increasing the Sn content in the IQC matrix, as discerned from Figure 6.

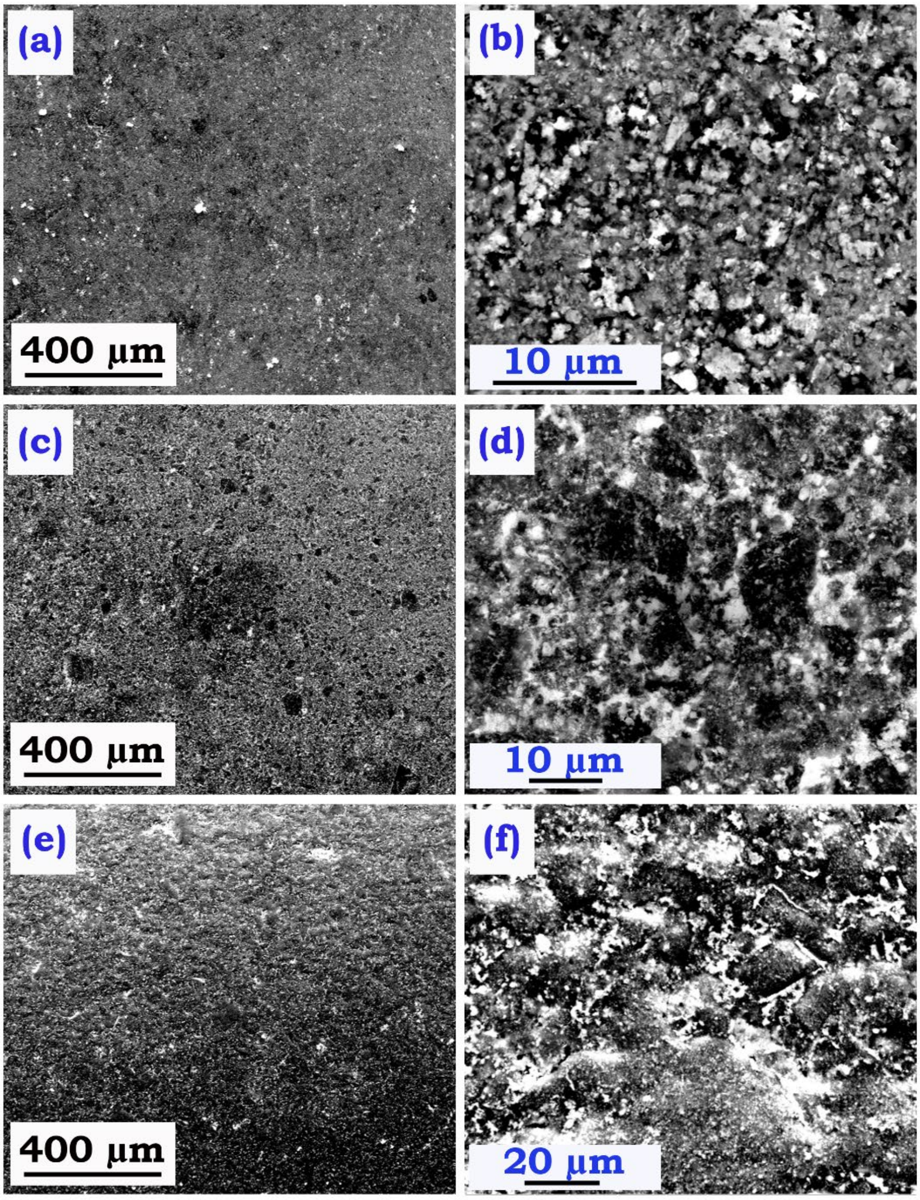

Figure 6. SEM micrograph of (**a**,**b**) IQC-10Sn-PS, (**c**,**d**) IQC-20Sn-PS, (**e**,**f**) IQC-30Sn-PS pressureless-sintered at 800 °C (1073 K) for 10 h at different magnifications.

Attempts were also made to investigate the formation of bulk IQC-10Sn-HP composite through hot pressing at 650 °C (923 K) and subsequently annealing at 800 °C (1073 K) for 4 h (IQC-10Sn-HPA). The microstructural features for the IQC-10Sn-HP hot-pressed and IQC-10Sn-HPA hot-pressed-plus-annealed composite are shown in Figure 7a–d, respectively.

The phase formation in the IQC-10Sn-HP and IQC-10Sn-HPA hot-pressed composite was similar to that of the pressureless-sintered samples. The optical micrograph shows the uniform distribution of Sn reinforcement particles in the IQC matrix. The indentation was carried out at different loads for the IQC-10Sn-HP and IQC-10Sn-HPA hot-pressed composite compared to the pressureless-sintered composite, as shown in Figure 8a,b. In both conditions, the indentation size effect (ISE) was evident. However, in the case of the hot-pressed samples, the ISE can be seen only up to the load of ~100 g. In case of pressureless sintering, ISE was evident up to a load of ~200 g.

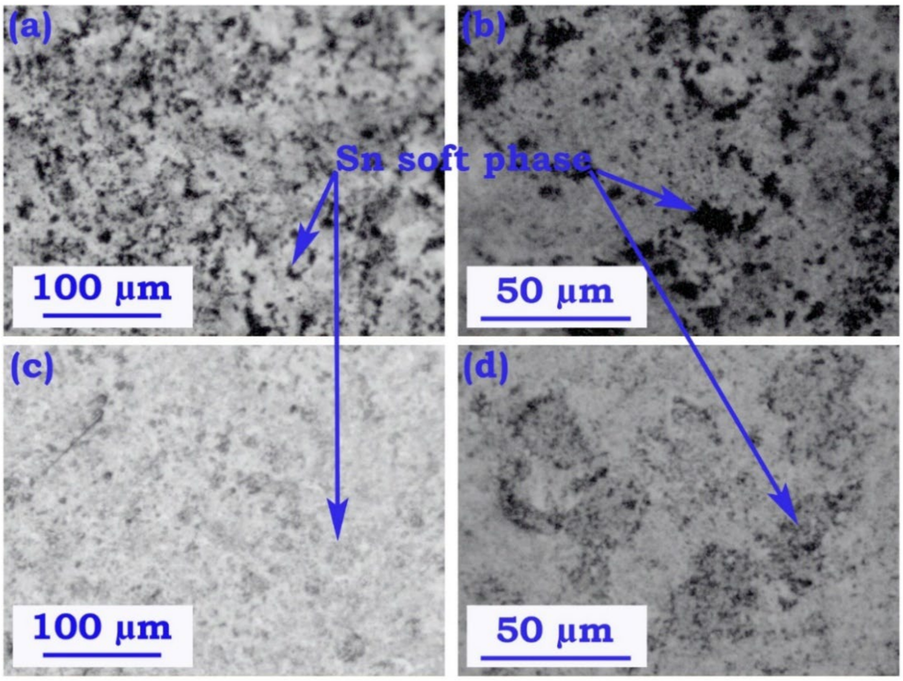

Figure 7. Optical micrograph of (**a**,**b**) IQC-10Sn hot-pressed at 650 °C (1073 K) for 15 min (IQC-10Sn-HP); (**c**,**d**) IQC-10Sn hot-pressed (650 °C) and annealed 800 °C for 4 h (IQC-10Sn-HPA).

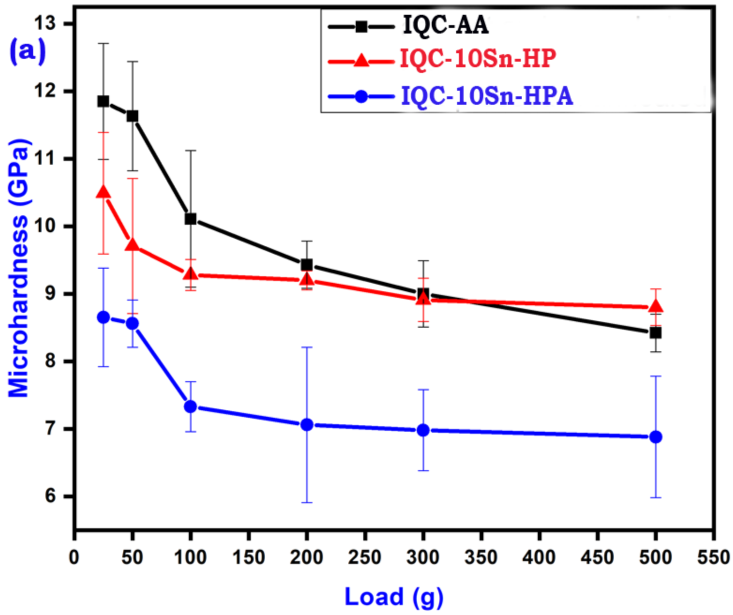

Figure 8. *Cont.*

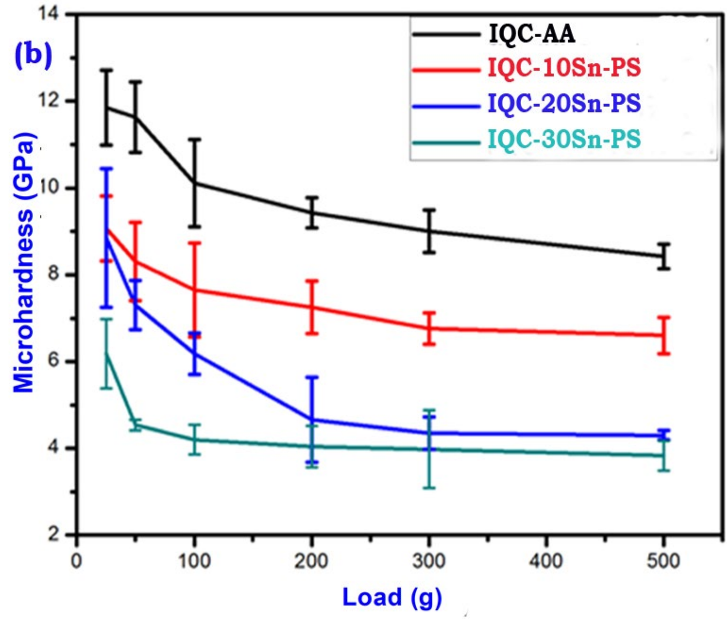

Figure 8. Microhardness value of (**a**) hot-pressed (IQC-10Sn-HP and IQC-10Sn-HPA) and (**b**) pressureless-sintered IQC-Sn bulk composite (IQC-10Sn-PS, IQC-20Sn-PS and IQC-30Sn-PS) at different indentation loads.

The ISE was observed mainly due to the elastic recovery and lower tendency for crack formation at small indentation loads. Increasing the indentation load above a specific limit, the bulk composite microhardness becomes constant (Figure 8a,b). The physical and mechanical properties of IQC-Sn composites prepared by pressureless sintering and hot pressing are mentioned in Table 2. The microhardness for hot-pressed (IQC-10Sn-HP) and hot-pressed + annealed (IQC-10Sn-HPA) composite was ~9.2 GPa and ~7.1 Gpa, respectively, at an indentation load of 200 g. On the other hand, the pressureless-sintered bulk composite shows a minor decrease in the microhardness (Figure 8b). The microhardness for IQC-10Sn-PS, IQC-20Sn-PS and IQC-30Sn-PS was ~7.2 GPa, 4.7 GPa and 4.1 GPa at an indentation load of 200 g. The lower microhardness of the pressureless-sintered compact may be attributed to the sintering mechanism in contrast to the hot-pressed samples. However, the relative density of IQC-Sn pressureless-sintered samples was found to increase with the content of Sn reinforcement (Table 2). This may be attributed to an increase in the propensity of liquid-phase sintering due to the content of Sn particles.

Table 2. Physical and mechanical properties of IQC-Sn-sintered composites.

Sample Designation	Processing Condition	Density			Microhardness (at 200 g) in GPa
		Experimental Density ($g.cm^{-3}$)	Theoretical Density ($g.cm^{-3}$)	Relative Density (%)	
IQC-AA	As-cast and annealed	4.19	-	-	~9.5
IQC-10Sn-PS	Pressureless sintering (PS)	2.78	4.49	~62	~7.2
IQC-20Sn-PS	Pressureless sintering (PS)	3.25	4.81	~68	~4.7
IQC-30Sn-PS	Pressureless sintering (PS)	3.77	5.11	~74	~4.1
IQC-10Sn-HP	Hot pressing (HP)	4.13	4.49	~92	~9.2
IQC-10Sn-HPA	Hot pressing and annealing (HPA)	4.18	4.49	~93	~7.1

Further efforts were also made to investigate the fracture toughness of the as-cast-plus-annealed IQC (IQC-AA) and IQC-10Sn-HP and IQC-10Sn-HPA hot-pressed composites.

For evaluating the fracture toughness of these materials, the Palmqvist method [53,54] was used. The fracture toughness of any brittle material can be computed by using Equation (3), as mentioned below:

$$K_{IC} = 0.035 * \Phi^{\left(-\frac{3}{5}\right)} * H * \left(\frac{d/2}{\sqrt{l}}\right) * \left(\frac{H}{E}\right)^{\left(-\frac{2}{5}\right)} \quad (3)$$

where K_{IC} = fracture toughness, Φ = constraint factor, H = microhardness, E = Young's modulus, d = diagonal length of indentation, L = total length of the Palmqvist crack.

The various factors considered for computing the fracture toughness using the Palmqvist crack method are reported elsewhere [55,56]. The fracture toughnesses of the as-cast-plus-annealed IQC (IQC-AA), and IQC-10Sn-HP and IQC-10Sn-HPA hot-pressed composite are mentioned in Table 3. The increase in the fracture toughness of the IQC-10Sn-HP and IQC-10Sn-HPA hot-pressed composite can be attributed to the inhibition of cracks due to soft Sn reinforcement particles. From Figure 9a–g, it can be discerned that the length of the crack in IQC is ~10 times more than that observed for IQC-10Sn-HP and IQC-10Sn-HPA hot-pressed composite. A significant increase in the fracture toughness of these composites is observed, as shown in Table 3.

Table 3. Fracture toughness of IQC-Sn hot-pressed composite.

Sample Specification	Fracture Toughness MPa. (m)$^{1/2}$	Enhancement (%)
As cast and annealed (IQC-AA)	1.58 ± 0.27	–
IQC-10Sn-HP	1.92 ± 0.12	22%
IQC-10Sn-HPA	1.81 ± 0.16	15%

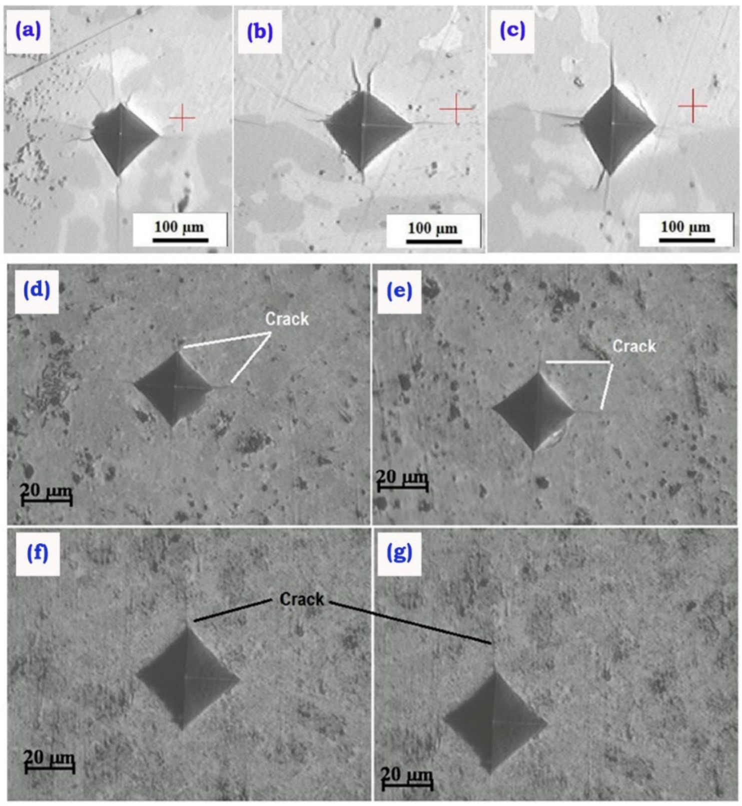

Figure 9. Optical micrograph showing indentation marks on (**a**) as-cast and annealed IQC (IQC-AA) at a load of 200 g and (**b**,**c**) as-cast and annealed IQC (IQC-AA) at a load 500 g. Optical micrograph showing indentation cracks in IQC-10Sn composite at a load of 500 g: (**d**,**e**) hot-pressed at 650 °C (923 K) (IQC-10Sn-HP) and (**f**,**g**) hot-pressed at 650 °C (923 K) followed by annealing at 800 °C 1023 K) (IQC-10Sn-HPA).

4. Discussions

The lucrative and exciting structural and functional properties of Al-Cu-Fe IQC make them potential materials for coatings and/or reinforcement in the Al-matrix composites. The excellent wear resistance and low coefficient of friction of Al-Cu-Fe IQC make them suitable for coating applications [10,57]. However, the room-temperature brittleness restricts its usage for engineering applications. These Al-Cu-Fe IQC can be toughened either by nanostructuring [25] or by reinforcing soft phases such as Sn or Pb in the IQC matrix [20,30,31,47]. The present work discusses a hybrid strategy for toughening IQC by synthesizing Sn-reinforced Al-Cu-Fe IQC matrix nanocomposites through milling. This hybrid strategy helps overcome the limitation pertaining to the difference in the melting point of Sn and IQC matrix when prepared through melting and solidification. In our previous investigation, the synthesis of IQC-Sn nanocomposites has shown the homogenous distribution of Sn reinforcement in the IQC matrix [49]. The structural transformation in these IQC-Sn milled powders can be attributed to phason strain induced in Al-Cu-Fe IQC during MM only [49]. A few researchers have reported the structural transformation of IQC during MM due to contamination of Fe and Cr from the milling vials and balls consisting of steel [43,58]. In the present investigation, milling was conducted in WC vials and with WC balls to avoid the possibility of structural transformation due to chemical contamination.

In the past two decades, Nicula and his coworkers have made considerable efforts to understand the consolidation behavior of the Al-Cu-Fe IQC phase during spark-plasma sintering (SPS) [59–61]. Further, many researchers have evaluated the mechanical properties and fracture toughness after nonequilibrium sintering of Al-Cu-Fe IQC alloys having a relative density >99.00% [62]. In a detailed investigation, Fleury et al. [62] observed the SPSed Al-Cu-Fe IQC phase having a microhardness in the range of 7.75–8.90 GPa. The microhardness variation depended on the phases that evolved during the sintering at different temperatures. In the present investigation, the microhardness for the IQC-Sn nanocomposite powders and bulk composite was found comparable to Al-Cu-Fe IQC prepared by SPS (as reported in Table 1). The high microhardness of IQC-Sn composite (~7.3 GPa) was attributed to grain refinement and the homogenous distribution of Sn reinforcement in the nanocomposite powder (Figure 3 and Table 1). The pure IQC milled at different milling intensities has the almost same microhardness as that of the IQC-10Sn [42]. The MM technique is instrumental in synthesizing IQC-Sn nanocomposite powder.

The bulk IQC-Sn composite prepared by pressureless sintering and hot pressing shows a significant rise in the microhardness and fracture toughness (Figures 8 and 9 and Table 2). The microhardness of as-cast and annealed IQC (IQC-AA) was found to be ~9.5 GPa at a load of 200 g. However, the microhardness of the IQC-Sn composite was slightly lower in comparison to IQC. An investigation by Srivastava et al. [20] used spray forming to produce IQC matrix composite reinforced with 10 wt % Sn having a microhardness of ~6.0 GPa. The microhardness of the IQC without Sn was found to be ~9.3 GPa. The nominal decrease in the microhardness was attributed due to soft Sn particulates in IQC matrix. The values of microhardness in the present investigation were also in line with the findings of Srivastava et al. [20].

The considerable increase in fracture toughness was attributed to the soft Sn particles that restrict cracks propagation, as described in the detailed work by Srivastava et al. [20]. In the present investigation, due to the implication of hybrid strategy (i.e., nanostructuirng and homogenous distribution of Sn) for the toughening of IQC, an enormous increase in the microhardness having synergy with fracture toughness was evident (Figures 8 and 9, Tables 2 and 3). Due to homogenous distribution and liquid-phase sintering of Sn particles in the IQC matrix (Figures 8 and 9) during MM, pressureless sintering and hot pressing, significant enhancement in the microhardness of IQC-Sn composites was observed in contrast to those reported by other investigators [20,44,47]. The high microhardness and fracture toughness of the IQC-Sn nanocomposite powder and the bulk composite may help design coating material for engineering applications.

5. Conclusions

The structural transformation of IQC-Sn nanocomposite powder as a function of milling duration and volume fraction of Sn have been analyzed. The sequence of structural changes was co-related with the microhardness of IQC-Sn nanocomposite powder milled up to 40 h. Further, efforts were made to study the microstructure and toughening behavior of bulk IQC-Sn composite prepared by pressureless sintering and hot pressing. The following conclusions can be made from the present investigations:

1. After milling, the Al-Cu-Fe IQC phase transforms to the $Al_{13}Fe_4$ and B2-type Al (Cu, Fe) phases. However, the phase fraction of $Al_{13}Fe_4$ and B2-type phases formed after MM is dependent on the volume fraction of Sn reinforcement in the IQC-Sn nanocomposite powder.
2. The structural transformation and grain refinement induced during milling affect the indentation behavior and microhardness of IQC-Sn nanocomposite powders. The microhardness in these milled powders can be tuned in the range of ~5.2 to 7.3 GPa.
3. The IQC-Sn bulk composite prepared through hot pressing increases microhardness and fracture toughness.
4. The microhardness of the hot-pressed sample (IQC-10Sn-HP) at 200 g load was found to be ~9.2 GPa. However, the pressureless-sintered composite has a lower microhardness value than that of the hot-pressed sample at a 200 g load.
5. The overall increase in the fracture toughness of IQC-10Sn-HP composite was ~22% due to the significant reduction in the indentation crack length (~15 μm). This reduction in the crack length was attributed to Sn particles' homogenous distribution in the IQC matrix, enhancing its propensity to arrest the cracks. This offers the possibility of synthesizing nanocomposite powders and bulk composite by HP and pressureless sintering, having an optimal combination of microhardness and fracture toughness required as feedstock for coating applications.

Supplementary Materials: The following supporting information can be downloaded at: https://www.mdpi.com/article/10.3390/jmmp6030060/s1, Table S1: Sample designation and processing conditions of IQC-Sn composites.

Author Contributions: Conceptualization, Y.S. and N.K.M.; methodology, Y.S. and V.S.; software, Y.S. and V.S.; validation, Y.S.; formal analysis, Y.S. and N.K.M.; investigation, Y.S.; resources, K.C. and N.K.M.; data curation, Y.S. and V.S.; writing—original draft preparation, Y.S.; writing—review and editing, K.C. and N.K.M.; visualization, Y.S. and V.S.; supervision, N.K.M.; project administration, N.K.M. All authors have read and agreed to the published version of the manuscript.

Funding: This research received no external funding.

Data Availability Statement: The data present in this study available on reasonable request to corresponding authors. The present data forms the part of ongoing study and therefore not shared publicly.

Acknowledgments: The authors would like to thank S. Lele, R. K. Mandal, and J. Basu for many stimulating discussion. Authors acknowledge support and guidance of R Manna for extending the hot-pressing facility. The Central Instrument Facility, IIT (BHU) is thankfully acknowledged for providing the necessary characterization facility. The authors also acknowledge DST-FIST (Level-II) for infrastructural support. The authors would like to thank K. G. Prashanth for the invitation to contribute this article to the special issue of the Journal of Manufacturing and Materials Processing.

Conflicts of Interest: Authors declare no conflict of interest.

References

1. Shechtman, D.; Blech, I.; Gratias, D.; Cahn, J.W. Metallic Phase with Long-Range Orientational Translational Symmetry. *Phys. Rev. Lett.* **1984**, *53*, 1951–1954. [CrossRef]
2. Pandey, V.K.; Shadangi, Y.; Shivam, V.; Sarma, B.; Mukhopadhyay, N. Theoretical and experimental study on phase stability of TiVZrMoW refractory high entropy alloy. *Philos. Mag.* **2021**, *102*, 480–503. [CrossRef]
3. Singh, N.; Shadangi, Y.; Goud, G.S.; Pandey, V.K.; Shivam, V.; Mukhopadhyay, N.K. Fabrication of MgAlSiCrFe Low-Density High-Entropy Alloy by Mechanical Alloying and Spark Plasma Sintering. *Trans. Indian Inst. Met.* **2021**, *74*, 2203–2219. [CrossRef]

4. Mukhopadhyay, N.; Belger, A.; Paufler, P.; Kim, D. Nanoindentation studies on Cu–Ti–Zr–Ni–Si–Sn bulk metallic glasses. *Mater. Sci. Eng. A* **2007**, *449–451*, 954–957. [CrossRef]
5. Chaubey, A.; Scudino, S.; Khoshkhoo, M.S.; Prashanth, K.; Mukhopadhyay, N.; Mishra, B.; Eckert, J. High-strength ultrafine grain Mg–7.4%Al alloy synthesized by consolidation of mechanically alloyed powders. *J. Alloys Compd.* **2014**, *610*, 456–461. [CrossRef]
6. Chaubey, A.K.; Scudino, S.; Khoshkhoo, M.S.; Prashanth, K.G.; Mukhopadhyay, N.K.; Mishra, B.K.; Eckert, J. Synthesis and Characterization of NanocrystallineMg-7.4%Al Powders Produced by Mechanical Alloying. *Metals* **2013**, *3*, 58–68. [CrossRef]
7. Huttunen-Saarivirta, E. Microstructure, fabrication and properties of quasicrystalline Al–Cu–Fe alloys: A review. *J. Alloys Compd.* **2004**, *363*, 154–178. [CrossRef]
8. Huttunen-Saarivirta, E.; Turunen, E.; Kallio, M. Microstructural characterisation of thermally sprayed quasicrystalline Al–Co–Fe–Cr coatings. *J. Alloys Compd.* **2003**, *354*, 269–280. [CrossRef]
9. Mukhopadhyay, N.K.; Yadav, T.P. Quasicrystals: A New Class of Structurally Complex Intermetallics. *J. Indian Inst. Sci.* **2022**, 1–32. [CrossRef]
10. Yadav, T.; Mukhopadhyay, N. Quasicrystal: A low-frictional novel material. *Curr. Opin. Chem. Eng.* **2018**, *19*, 163–169. [CrossRef]
11. Dubois, J.-M. Properties- and applications of quasicrystals and complex metallic alloys. *Chem. Soc. Rev.* **2012**, *41*, 6760–6777. [CrossRef] [PubMed]
12. Yadav, T.; Mukhopadhyay, N.; Tiwari, R.; Srivastava, O. Studies on the formation and stability of nano-crystalline $Al_{50}Cu_{28}Fe_{22}$ alloy synthesized through high-energy ball milling. *Mater. Sci. Eng. A* **2005**, *393*, 366–373. [CrossRef]
13. Srivastava, V.C.; Uhlenwinkel, V.; Schulz, A.; Zoch, H.-W.; Mukhopadhyay, N.K.; Chowdhury, S.G. Synthesis of single phase i-AlCuFe bulk quasicrystal by spray forming. *Z. Krist.* **2008**, *223*, 711–715. [CrossRef]
14. Yadav, T.; Mishra, S.; Pandey, S.; Singh, D.; Lowe, M.; Tamura, R.; Mukhopadhyay, N.; Srivastava, O.; McGrath, R.; Sharma, H. Leaching of Al-Based Polygrain Quasicrystalline and Related Crystalline Surfaces. *Acta Phys. Pol. A* **2014**, *126*, 629–632. [CrossRef]
15. Steurer, W.; Deloudi, S. *Crystallography of Quasicrystals*, 1st ed.; Springer: Berlin/Heidelberg, Germany, 2009.
16. Stagno, V.; Bindi, L.; Shibazaki, Y.; Tange, Y.; Higo, Y.; Mao, H.-K.; Steinhardt, P.; Fei, Y. Icosahedral AlCuFe quasicrystal at high pressure and temperature and its implications for the stability of icosahedrite. *Sci. Rep.* **2014**, *4*, 5869. [CrossRef] [PubMed]
17. Bindi, L.; Steinhardt, P.J.; Yao, N.; Lu, P.J. Natural Quasicrystals. *Science* **2009**, *324*, 1306–1309. [CrossRef]
18. Mukhopadhyay, N.K.; Ranganathan, S.; Chattopadhyay, K. Evolution of superlattice order in Al–Mn quasicrystals and its relation to face-centred icosahedral quasicrystals. *Philos. Mag. Lett.* **1989**, *60*, 207–211. [CrossRef]
19. Tsai, A.-P.; Inoue, A.; Masumoto, T. Preparation of a new Al-Cu-Fe quasicrystal with large grain sizes by rapid solidification. *J. Mater. Sci. Lett.* **1987**, *6*, 1403–1405. [CrossRef]
20. Srivastava, V.; Huttunen-Saarivirta, E.; Cui, C.; Uhlenwinkel, V.; Schulz, A.; Mukhopadhyay, N. Bulk synthesis by spray forming of Al–Cu–Fe and Al–Cu–Fe–Sn alloys containing a quasicrystalline phase. *J. Alloys Compd.* **2014**, *597*, 258–268. [CrossRef]
21. Shadangi, Y.; Sharma, S.; Shivam, V.; Basu, J.; Chattopadhyay, K.; Majumdar, B.; Mukhopadhyay, N. Fabrication of Al–Cu–Fe quasicrystal reinforced 6082 aluminium matrix nanocomposites through mechanical milling and spark plasma sintering. *J. Alloys Compd.* **2020**, *828*, 154258. [CrossRef]
22. Yadav, T.P.; Woellner, C.F.; Sharifi, T.; Sinha, S.K.; Qu, L.-L.; Apte, A.; Mukhopadhyay, N.K.; Srivastava, O.N.; Vajtai, R.; Galvão, D.S.; et al. Extraction of Two-Dimensional Aluminum Alloys from Decagonal Quasicrystals. *ACS Nano* **2020**, *14*, 7435–7443. [CrossRef] [PubMed]
23. Yadav, T.P.; Woellner, C.F.; Sinha, S.K.; Sharifi, T.; Apte, A.; Mukhopadhyay, N.K.; Srivastava, O.N.; Vajtai, R.; Galvao, D.S.; Tiwary, C.S.; et al. Liquid Exfoliation of Icosahedral Quasicrystals. *Adv. Funct. Mater.* **2018**, *28*, 1801181. [CrossRef]
24. Mishra, S.; Yadav, T.; Mukhopadhyay, N.; Srivastava, O. Synthesis of fine skeletal structure on Al–Cu–Co decagonal quasicrystals for hydrogen production through steam reforming of methanol. *Int. J. Hydrogen Energy* **2020**, *45*, 24491–24501. [CrossRef]
25. Mukhopadhyay, N.K.; Ali, F.; Scudino, S.; Khoshkhoo, M.S.; Stoica, M.; Srivastava, V.C.; Uhlenwinkel, V.; Vaughan, G.; Suryanarayana, C.; Eckert, J. Grain size softening effect in $Al_{62.5}Cu_{25}Fe_{12.5}$ nanoquasicrystals. *Appl. Phys. Lett.* **2013**, *103*, 201914. [CrossRef]
26. Rawat, R.; Tiwari, A.; Arun, N.; Rao, S.N.; Pathak, A.; Shadangi, Y.; Mukhopadhyay, N.; Tripathi, A. Nanosecond pulsed laser ablation of Al–Cu–Fe quasicrystalline material: Effects of solvent and fluence. *J. Alloys Compd.* **2020**, *859*, 157871. [CrossRef]
27. Singh, A.; Tsai, A.P. Melting behaviour of lead and bismuth nano-particles in quasicrystalline matrix—The role of interfaces. *Sadhana Acad. Proc. Eng. Sci.* **2003**, *28*, 63–80. [CrossRef]
28. Singh, A.; Somekawa, H.; Matsushita, Y.; Tsai, A. Solidification of tin on quasicrystalline surfaces. *Philos. Mag.* **2012**, *92*, 1106–1128. [CrossRef]
29. Singh, A.; Tsai, A. Heterogeneous nucleation of lead on quasicrystals. *Philos. Mag. Lett.* **1998**, *77*, 89–94. [CrossRef]
30. Yadav, T.; Singh, D.; Tiwari, R.; Srivastava, O. Enhanced microhardness of mechanically activated carbon–quasicrystal composite. *Mater. Lett.* **2012**, *80*, 5–8. [CrossRef]
31. Patiño-Carachure, C.; Flores-Chan, J.; Gil, A.F.; Rosas, G. Synthesis of onion-like carbon-reinforced AlCuFe quasicrystals by high-energy ball milling. *J. Alloys Compd.* **2016**, *694*, 46–50. [CrossRef]
32. Tsai, A. Metallurgy of Quasicrystals: Alloys and Preparation. *MRS Bull.* **1997**, *22*, 43–47. [CrossRef]
33. Barua, P.; Murty, B.; Srinivas, V. Mechanical alloying of Al–Cu–Fe elemental powders. *Mater. Sci. Eng. A* **2001**, *304–306*, 863–866. [CrossRef]

34. Murty, B.; Barua, P.; Srinivas, V.; Schurack, F.; Eckert, J. Synthesis of $(Al_{65}Cu_{20}Fe_{15})100-xSix$ quasicrystalline alloys by mechanical alloying. *J. Non-Cryst. Solids* **2004**, *334–335*, 44–47. [CrossRef]
35. Barua, P.; Murty, B.S.; Mathur, B.K.; Srinivas, V. On icosahedral phase formation in mechanically alloyed $Al_{70}Cu_{20}Fe_{10}$. *Mater. Sci. Eng. A* **2000**, *294–296*, 65–67. [CrossRef]
36. Yadav, T.; Mukhopadhyay, N.; Tiwari, R.; Srivastava, O. On the evolution of quasicrystalline and crystalline phases in rapidly quenched Al-Co–Cu–Ni alloy. *Mater. Sci. Eng. A* **2007**, *449–451*, 1052–1056. [CrossRef]
37. Mukhopadhyay, N.K.; Yadav, T.P.; Tiwari, R.S.; Srivastava, O.N. Synthesis of nanocrystalline spinel phase by mechanical milling of Al–Cu–Fe and Al–Cu–Cr–Fe quasicrystalline alloys. *Z. Krist.* **2008**, *223*, 716–720. [CrossRef]
38. Mukhopadhyay, N.K.; Yadav, T.P. Some Aspects of Stability and Nanophase Formation in Quasicrystals during Mechanical Milling. *Isr. J. Chem.* **2011**, *51*, 1185–1196. [CrossRef]
39. Barua, P.; Srinivas, V.; Murty, B.S. Synthesis of quasicrystalline phase by mechanical alloying of $Al_{70}Cu_{20}Fe_{10}$. *Philos. Mag. A* **2000**, *80*, 1207–1217. [CrossRef]
40. Schurack, F.; Eckert, J.; Schultz, L. Synthesis and mechanical properties of mechanically alloyed Al-Cu-Fe quasicrystalline composites. *Philos. Mag.* **2003**, *83*, 1287–1305. [CrossRef]
41. Tiwari, R.S.; Yadav, T.P.; Mukhopadhyay, N.K.; Abu Shaz, M.; Srivastava, O.N. Nanocrystallization and structural correlation in quasicrystalline and crystalline phases during mechanical milling. *Z. Krist.* **2009**, *224*, 26–30. [CrossRef]
42. Ali, F.; Scudino, S.; Gorantla, S.; Srivastava, V.; Shahid, H.; Uhlenwinkel, V.; Stoica, M.; Vaughan, G.; Mukhopadhyay, N.; Eckert, J. Mechanically driven phase transformation in single phase $Al_{62.5}Cu_{25}Fe_{12.5}$ quasi-crystals: Effect of milling intensity. *Acta Mater.* **2013**, *61*, 3819–3830. [CrossRef]
43. Mukhopadhyay, N.K.; Yadav, T.P.; Srivastava, O.N. Effects of ball milling and annealing of an alloy in the Al-Fe-Cu system: Implications for phase equilibria. *Philos. Mag. Lett.* **2003**, *83*, 423–432. [CrossRef]
44. Fleury, E.; Kim, Y.-C.; Kim, D.-H.; Kim, W.-T. The toughening of Al–Cu–Fe(-B) quasicrystals by Sn particles. *J. Non-Cryst. Solids* **2004**, *334–335*, 449–452. [CrossRef]
45. Shao, T.; Cao, X.; Fleury, E.; Kim, D.-H.; Hua, M.; Se, D. Tribological behavior of plasma sprayed Al–Cu–Fe+Sn quasicrystalline composite coatings. *J. Non-Cryst. Solids* **2004**, *334–335*, 466–470. [CrossRef]
46. Singh, A.; Somekawa, H.; Tsai, A. Interfaces made by tin with icosahedral phase matrix. *Scr. Mater.* **2008**, *59*, 699–702. [CrossRef]
47. Mukhopadhyay, N.K.; Uhlenwinkel, V.; Srivastava, V.C. Synthesis and Characterization of Bulk Al-Cu-Fe Based Quasicrystals and Composites by Spray Forming. *J. Mater. Eng. Perform.* **2015**, *24*, 2172–2178. [CrossRef]
48. Shadangi, Y.; Shivam, V.; Singh, M.K.; Chattopadhyay, K.; Basu, J.; Mukhopadhyay, N. Synthesis and characterization of Sn reinforced Al-Cu-Fe quasicrystalline matrix nanocomposite by mechanical milling. *J. Alloys Compd.* **2019**, *797*, 1280–1287. [CrossRef]
49. Shadangi, Y.; Shivam, V.; Varalakshmi, S.; Basu, J.; Chattopadhyay, K.; Majumdar, B.; Mukhopadhyay, N. Mechanically driven structural transformation in Sn reinforced Al–Cu–Fe quasicrystalline matrix nanocomposite. *J. Alloys Compd.* **2020**, *834*, 155065. [CrossRef]
50. Singh, N.; Shadangi, Y.; Mukhopadhyay, N.K. Phase Evolution and Thermal Stability of Low-Density MgAlSiCrFe High-Entropy Alloy Processed Through Mechanical Alloying. *Trans. Indian Inst. Met.* **2020**, *73*, 2377–2386. [CrossRef]
51. Singh, N.; Shadangi, Y.; Shivam, V.; Mukhopadhyay, N.K. MgAlSiCrFeNi low-density high entropy alloy processed by mechanical alloying and spark plasma sintering: Effect on phase evolution and thermal stability. *J. Alloys Compd.* **2021**, *875*, 159923. [CrossRef]
52. Pandey, V.K.; Shadangi, Y.; Shivam, V.; Basu, J.; Chattopadhyay, K.; Majumdar, B.; Sarma, B.N.; Mukhopadhyay, N.K. Synthesis, Characterization and Thermal Stability of Nanocrystalline MgAlMnFeCu Low-Density High-Entropy Alloy. *Trans. Indian Inst. Met.* **2020**, *74*, 33–44. [CrossRef]
53. Murthy, G.V.S.; Ray, A.K.; Minz, R.K.; Mukhopadhyay, N.K. Microhardness and Fracture Toughness Studies of Decagonal Quasicrystal in Al-Cu-Co System. *J. Mater. Sci. Lett.* **1999**, *18*, 255–258. [CrossRef]
54. Mukhopadhyay, N.K.; Paufler, P. Micro- and nanoindentation techniques for mechanical characterisation of materials. *Int. Mater. Rev.* **2006**, *51*, 209–245. [CrossRef]
55. Köster, U.; Liebertz, H.; Liu, W. Plastic deformation of quasi-crystalline and crystalline phases in AlCuFe alloys. *Mater. Sci. Eng. A* **1994**, *181–182*, 777–780. [CrossRef]
56. Köster, U.; Liu, W.; Liebertz, H.; Michel, M. Mechanical properties of quasicrystalline and crystalline phases in AlCuFe alloys. *J. Non-Cryst. Solids* **1993**, *153–154*, 446–452. [CrossRef]
57. Kang, S.; Dubois, J.; von Stebut, J. Tribological properties of quasicrystalline coatings. *J. Mater. Res.* **1993**, *8*, 2471–2481. [CrossRef]
58. Mukhopadhyay, N.; Ali, F.; Srivastava, V.; Yadav, T.; Sakaliyska, M.; Surreddi, K.; Scudino, S.; Uhlenwinkel, V.; Eckert, J. Strain-induced structural transformation of single-phase Al–Cu–Fe icosahedral quasicrystal during mechanical milling. *Philos. Mag.* **2010**, *91*, 2482–2490. [CrossRef]
59. Nicula, R.; Turquier, F.; Stir, M.; Kodash, V.; Groza, J.; Burkel, E. Quasicrystal phase formation in Al–Cu–Fe nanopowders during field-activated sintering (FAST). *J. Alloys Compd.* **2007**, *434–435*, 319–323. [CrossRef]
60. Nicula, R.; Stir, M.; Turquier, F.; Burkel, E. Single-phase bulk Al–Cu–Fe quasicrystals by field-assisted sintering. *Mater. Sci. Eng. A* **2008**, *475*, 113–116. [CrossRef]
61. Nicula, R.; Ishizaki, K.; Stir, M.; Shen, Z.; Vaucher, S. Rapid synthesis and densification of single-phase Al–Cu–Fe quasicrystals by spark plasma sintering or microwave heating. *Philos. Mag.* **2010**, *91*, 2450–2457. [CrossRef]
62. Fleury, E.; Lee, J.H.; Kim, S.H.; Kim, W.T.; Kim, J.S.; Kim, D.H. Spark plasma sintering of Al-Si-Cu-Fe quasi-crystalline powder. *Met. Mater. Trans. A* **2003**, *34*, 841–849. [CrossRef]